NDT.net e-Journal of Nondestructive Testing - ISSN 1435-4934 - www.ndt.net
13th Conference on Industrial Computed Tomography, Wels, Austria (iCT 2024), www.ict-conference.com/2024

eJNDT

High Energy Computed Tomography of high-density alloys using a 6 MeV Linear Accelerator: detectability and use of Artificial Intelligence

Davide Borghi[1], Fabio Esposito[1], Stefano Benuzzi[1], Lionel Gay[2]

[1]TEC Eurolab srl, Viale Europa 40, Italy
e-mail: borghi@tec-eurolab.com, esposito@tec-eurolab.com, benuzzi@tec-eurolab.com, m.righi@tec-eurolab.com

[2]Safran Additive Manufacturing Campus (SAMC), V73R+26, 33185, Le Haillan, France
e-mail: lionel.gay@safrangroup.com

Abstract

In a sector not yet regulated like Additive Manufacturing, knowledge of the technology represents an important opportunity for companies that want to guarantee the quality of their 3D printing products. Furthermore, AM technologies are acquiring an increasing importance in the industrial production and in different fields, also using different materials, from polymeric to high density material such as Inconel. **[1]** Components made by this technology could have complex geometries and the combination with high density materials can compromise both the capability and overall quality of the process. **[2]** Industrial computed tomography is a widespread NDT technique that allows to perform a complete analysis, by combining dimensional inspection and a full volume defect control. **[3]** At this point, it is important to define the limit of this technology in terms of detection of defects and geometries. This case study will focus on the first topic looking for the detectability of anomalies within the components made by Titanium alloy (TA6V) with high thickness, adding some considerations about possible use of an Artificial Intelligence (AI) based software, using a powerful source such as a Linear Accelerator. Many experiments have been performed through different CT analysis techniques, some of them carried out at high resolution on small samples made in Titanium alloy (TA6V) by additive manufacturing, looking for the real shape of designed defects. Then, a scan of these samples was performed using the LINAC system. Moreover, the use of a trained AI allows optimization of NDT process, thus reducing the influence of the human factor. The results showed the reliability of the technique and procedure used, given that it is possible to detect defects even in the worst analysis condition as in this case. These results consider both human factor and quality parameters of a CT system.

Keywords: Defect Analysis, Artificial Intelligence, Linear Accelerator, High density alloy

1 Introduction

Industrial computed tomography (CT) has revolutionized the inspection of components with complex geometries, such as additive manufacturing (AM) parts. **[3]** However, due to the lack of standardized practices defining quality requirements for CT volumes, the use of Representative Quality Indicators (RQIs) becomes essential. **[4]** RQIs serve as validation tools for specific CT techniques, ensuring that they accurately represent the part's geometry and material properties. These indicators incorporate artificial or known discontinuities that are representative of the applicable acceptance criteria, enabling reliable and consistent quality assessment. Prior to its usage in production scans, RQIs must undergo validation using a high-resolution system to ensure the verification of the number and dimensions of real indications compared to the nominal indications. Once the RQI has been successfully validated, it can be employed, alongside the actual part, in production scans. It is worth noting that in the case of Additive Manufactured RQIs, the generated discontinuities are often "full of powder" and exhibit reduced contrast with the background material. **[5]**

An Additive Manufacturing Titanium Alloy Manifold (250mm x 180mm x 260mm) manufactured by SAFRAN Additive Manufacturing Campus according to Safran Landing System design was used for the study. To simulate a favorable condition, an RQI was strategically placed within the part. The part and RQI were scanned using the TEC Eurolab DIONDO D7 6.0 MeV LINAC System, with an approximate voxel size of 130 um. The primary goal was to compare the high-resolution scan of the RQI with the High Energy scan, which simulates representative discontinuities present in the part. A 6.0 MeV CT scan was performed on the Part + RQI using TEC Eurolab DIONDO D7 LINAC System. Despite having a larger voxel size and smaller magnification compared to micro-CT scans, many discontinuities were successfully detected and measurable in all three dimensions. Furthermore, the overall grey value of the part itself demonstrated good uniformity and minimal contribution from artifacts.

TEC Eurolab developed a customized and tailored software for the automatic detection of defects within additive manufacturing (AM) parts. This software utilizes input images captured through industrial computed tomography. The AI, trained specifically for this purpose, processes the images automatically and generates a comprehensive report that includes statistical information and identifies any anomalies detected. Operators can access a control dashboard through a web browser, allowing them to view the reports generated for each analyzed object. To further train the AI, operators can provide feedback on the automatically generated reports through the dashboard. This iterative process enhances the AI's ability to recognize imperfections and improves the results of subsequent automatic analyses. The AI algorithm has been trained using an extensive dataset comprising over 4 million images and more than 250,000 labelled defects.

https://doi.org/10.58286/29238

Through continuous learning and progressive refinement, the deep learning model has achieved an impressive reliability rate of over 95% in accurately identifying anomalies.

2 Materials and Methods

The aim of the first part of this work was to investigate the detectability of artificial defects imposed in a large high-density part when scanned with a high energy source such as a 6MeV Linear Accelerator. The defects were imposed in a small cube with 10mm side. The cube was then manually placed inside a larger part (Hydraulic Manifold). Both were made via Laser Beam Melting using TA6V, and both were supplied by Safran Landing Systems. More details on the on the components will be given later. To achieve this result, the following steps were performed:

- Micro-CT scan of the small RQI cube, with the aim to characterize the real internal defects and therefore to establish the ground truth;
- 6 MeV scan of the Hydraulic Manifold with the RQI cube placed inside one of its cavities;
- Comparison of the obtained CT volumes to assess qualitatively the detectability of the defects;
- Test of a CT volume merging technique to verify its effectiveness in image quality enhancement (eg. noise reduction)

The second part of the work was targeted to assess the applicability of Artificial Intelligence to automate the defect recognition in CT slices. To achieve this, CT cross section slices of thousands of components of the same part number, were exported as single images. These images were then acquired by the AI software, which stores them in application server to be analyzed. The software is based on a deep learning model that processes these images and is trained in multiple ways:

- By comparing its results with previous reports generated on the same components by human users;
- Through feedbacks given by users on the results that the AI produces on new samples

This training was performed through hundreds of hours spread on several months of validation from the human users of the AI output.

2.1 RQI Cube Characterization

The RQI test part was produced by Safran Landing Systems via Additive Manufacturing. The specimen was designed to contain several internal cavities with different sizes. An overview of the original design is given in Image 1.

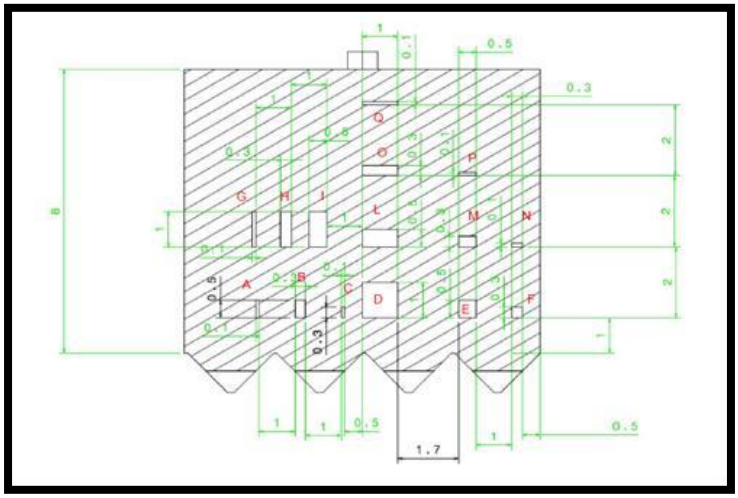

Figure 1 - Design of the RQI cube, cross section view. The dimensions are in millimetres. Designed by Safran Landing Systems

The artificial defects whom cross-section view is shown in Figure 1, extend 8mm in depth with 1mm spacing from the samples' faces.

It is known that producing an unsupported internal void via additive manufacturing often leads to irregularities in the down-skin area and, depending on the void geometry and size, some part could even collapse and fill the void **[6]**. Because of this, before proceeding with the High Energy scan, the RQI cube was scanned with a microfocus CT System by Safran. This first characterization was performed with a voxel size of 20µm, which gave the possibility to precisely characterize the defects that were produced in the real sample.

The CT cross sections obtained from the micro-CT scan are shown in Figure 2. From these images it is possible to check which voids were produced in the real RQI and with which "quality". The real sizes of the defects obtained by micro-CT are reported in Table 1. It can be noted that defects: C, N, O, P, Q are barely detectable or non-detectable, while other defects show sizes under the nominal ones. Considering the high scan quality (in terms of spatial resolution, noise, and lack of artifacts) it can be stated that the absence of these defects is probably due to them not actually being created or being collapsed during the printing process. This first characterization served the purpose of creating a "ground truth" on which the high energy scan can be compared with.

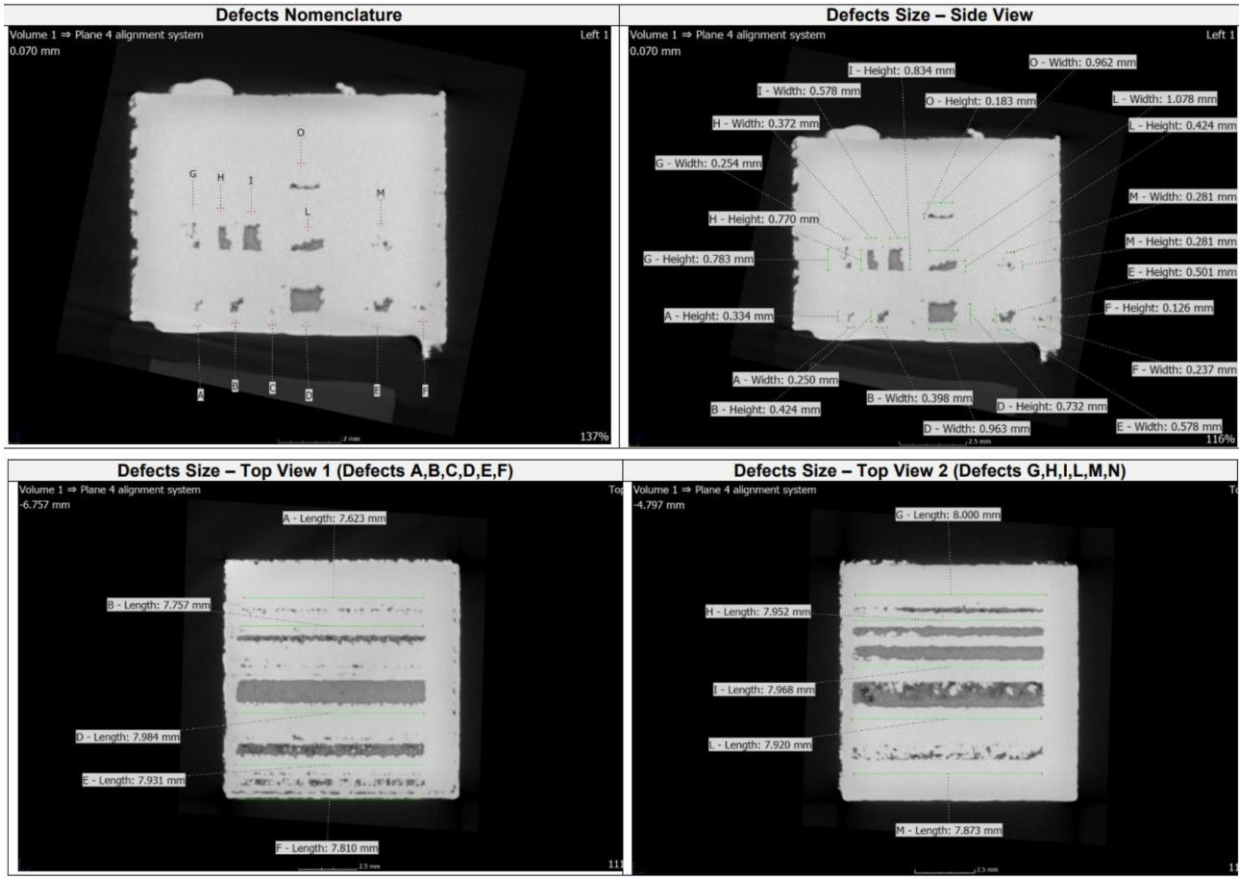

Figure 2 - CT sections of the RQI. top to bottom and left to right: Letters assigned to each void in side view; Measurement of the defect sizes in side view; Measurement of the depth in Top View for A,B,C,D,E,F; Measurement of the depth for G,H,I,L,M;

LETTER	CAD MEASUREMENTS (mm)			MICRO CT MEASUREMENTS (mm)			µCT REMARKS
	X	Y	LENGTH	X	Y	LENGTH	
A	0.1	0.5	8.0	0.25	0.33	7.62	Detectable
B	0.3	0.5	8.0	0.40	0.42	7.76	Detectable
C	0.1	0.3	8.0	--	--	--	Barely detectable
D	1.0	1.0	8.0	0.96	0.73	7.98	Detectable
E	0.5	0.5	8.0	0.58	0.50	7.93	Detectable
F	0.3	0.3	8.0	0.24	0.13	7.81	Detectable
G	0.1	1.0	8.0	0.25	0.78	8.00	Detectable
H	0.3	1.0	8.0	0.37	0.77	7.95	Detectable
I	0.5	1.0	8.0	0.58	0.83	7.97	Detectable
L	1.0	0.5	8.0	1.08	0.42	7.92	Detectable
M	0.5	0.3	8.0	0.28	0.28	7.87	Detectable
N	0.3	0.1	8.0	--	--	--	Not detectable
O	1.0	0.3	8.0	0.96	0.18	3.50	Partially detectable (only the central portion)
P	0.5	0.1	8.0	--	--	--	Not detectable
Q	1.0	0.1	8.0	--	--	--	Not detectable

Table 1 - RQI defects characterization: Size comparison between nominal and micro-CT measurements

2.2 Hydraulic manifold characteristics

It was chosen by Safran to use a part of their internal production as test specimen for the high energy scan. This part is produced through Laser Beam Melting of Titanium alloy (specifically TA6V) and features an intricate geometry, containing many internal ducts with thick and thin walls. On a low or medium energy system, these intersecting geometries would generate many streaking and beam hardening artifacts.

The part has a size of 250mm x 180mm x 260mm. Because of the overlapping of various internal geometries, depending on the part positioning during the CT scan, chords higher than 120mm must be penetrated by the X-Ray radiation. The Beer-Lambert law shows that such chord is not achievable with current 450 kV X-ray tube. A real test at 450kV performed by Safran confirmed it. Consequently, if the source energy is not high enough, this phenomenon leads to artifacts in the reconstructed volume, mainly coming from photon starvation and from beam hardening and scattering phenomena. **[2]** Because of this, it was chosen to use a 6MeV Linear Accelerator (Diondo D7 system) as the X-Ray source.

2.3 High Energy CT System Characteristics

TEC Eurolab is equipped with a CT system produced by Diondo (Diondo D7) featuring a Linear Accelerator X-Ray source. The source is a Siemens SILAC (Siemens Industrial Linear ACcelerator), capable of reaching 6 MeV of peak energy radiation. The detector is a Flat Panel Detector from Varex, model 4343HE DRZ HIGH with a 139µm pixel pitch and a 3k square matrix, resulting in a 417mm*417mm active area. The system is based on a granite manipulator, to guarantee dimensional stability. The source is also equipped with a lead collimator, which will be used to collimate the beam for scatter reduction. No collimator is present on the detector side.

2.4 Hydraulic Manifold Scan setup

As stated before, the choice went for a high energy system. Although this system has some unique advantages respect to lower energy ones, (mainly being higher penetration power, resulting in lower photon starvation and reduced beam hardening artefacts), we will start describing the similarities that is shares with common CT-systems, such as mini-focus systems (generally using a 450kV or 600kV energy source, that will be called in this article “medium” energy systems). In fact, just like it would have been done for a medium energy system, some scan setup techniques are shared:

- Sample positioning: the sample has to be tilted to and angle that both reduces the average global thickness to be penetrated by the x-rays, and also to avoid the “feldkamp artifact” on flat and horizontal surfaces **[7]**. The RQI cube was placed inside one of the cavities of the manifold, as shown in Figure 3:

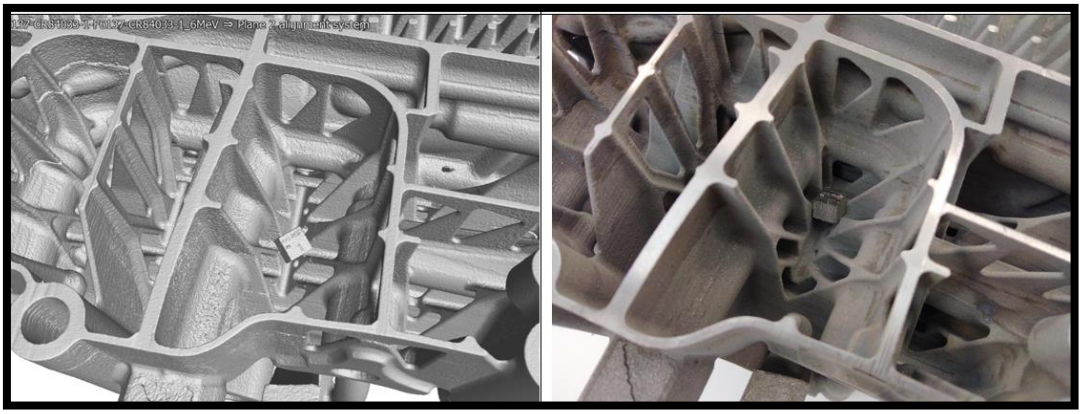

Figure 3 - RQI Cube position inside the complete manifold.

- Projection count: as for medium energy systems, the number of projections was set to be approximately 1.5 times ($\approx \pi/2$) the horizontal number of pixels occupied by the sample projection on the detector. **[7]**

When considering the advantages of this kind of system, as stated before, the higher penetration depth counts as the main one. However, this kind of energy spectra is more likely to cause scattering when hitting the sample part (and inside the detector elements too), which can result in higher Compton scattering influence in the projections **[1]**. Because of this, additional technical peculiarities must be considered in the scan setup:

- Source filtering: while it is true that the use of filters on the source can decrease the image contrast because it hardens the beam, it is necessary to consider that a linear accelerator produces a wide range of energy levels as the emitted spectrum is still produced by Bremsstrahlung phenomenon. **[8]** Consequently, to really take advantage of the highest energy part of this spectrum, thick source filtering is used, with a combination of lead and copper plates.
- Collimation: because of the higher energy level, also scattering artifact are more pronounced. These mainly occur inside the part itself, and inside the detector elements. **[9]** In order to reduce them, collimation of the beam has to be introduced. Specifically, the x-ray beam was horizontally collimated to about 10mm in height, while it was not collimated vertically.

The component was therefore scanned slice by slice in a "multi-line" or "narrow cone beam" configuration. This allowed, for each slice, to remove the scatter contribution from the whole component, and to limit it just to the thin slice scanned. Another approach to scatter reduction could have been to use an LDA (Linear Detector Array). **[10]** However, that would have meant an order of magnitude increase in scan time, and a reduction in resolution (given that the LDA detector that the system was equipped with, had a larger pixel pitch with respect to the flat panel detector). Because of this, it was decided to proceed with the Flat Panel Detector.

Moreover, the use of magnification also has to be considered in high energy CT: in fact, differently from microfocus and (to a lesser extent) from mini-focus systems, the characteristics of the source focal spot size (being in the order of magnitude of the millimetre) do not permit the use of high magnification factors **[11]**. In fact, if a magnification higher than 1.1-1.2 is used, geometrical blurring will have a significant influence on the acquired radiographs, reducing the global image sharpness. Depending on the sample size, achieving this low magnification, may or may not be possible.

The reconstruction of the volume was performed with the integrated software from the system manufacturer, which features a standard filtered back-projection algorithm with basic beam hardening correction. The reconstruction software is based on the Siemens Cera software package.

2.5 Scan Results

2.5.1 Complete Manifold volume overview

The obtained global volume had a pixel pitch of 130µm. The overall grey value turned out to be quite uniform and with low level of artifacts, therefore meeting Safran's quality standards. This is both thanks to the source filtering and to the narrow beam collimation. The 3D surface reconstruction indicates that this CT scan could have been used also for some metrology purposes, as the surface is determined without any major artifacts, although this is outside of the scope of this paper. However, it is not possible to share the images as an NDA is currently in place.

2.5.2 RQI volume region of interest overview

In order to assess the artificial defects detectability on the RQI cube, a reference system was built on it so that the CT slices were parallel to its faces. Using this views setup, the high energy scan of the RQI placed inside the manifold was compared to the micro-CT scan performed by Safran (which is taken as ground truth). The defects detectability evaluation is summarized in Table 2:

LETTER	MICRO CT MEASUREMENTS (mm)			HIGH ENERGY MEASUREMENTS			HIGH ENERGY REMARKS
	X	Y	LENGTH	X	Y	LENGTH	
A	0.25	0.33	7.62	--	--	--	Not detectable
B	0.40	0.42	7.76	0.6	0.5	7.0	Only detectable in "Merged" Scan
C	--	--	--	--	--	--	Not detectable
D	0.96	0.73	7.98	1.0	0.8	8.2	Detectable
E	0.58	0.50	7.93	0.7	0.6	7.9	Detectable
F	0.24	0.13	7.81	--	--	--	Not detectable
G	0.25	0.78	8.00	0.5	0.6	7.1	Only barely detectable in "merged" Scan
H	0.37	0.77	7.95	0.5	0.9	7.4	Detectable
I	0.58	0.83	7.97	0.6	0.9	7.4	Detectable
L	1.08	0.42	7.92	1.1	0.5	8.0	Detectable
M	0.28	0.28	7.87	--	--	--	Not detectable
N	--	--	--	--	--	--	Not detectable
O	0.96	0.18	3.50	0.9	0.6	1.6	Only barely detectable in "merged" Scan
P	--	--	--	--	--	--	Not detectable
Q	--	--	--	--	--	--	Not detectable

Table 2 - RQI defects detectability in high energy scan compared to defects detectability in micro-ct scan

The remarks on the right column of Table 2 show that the RQI defects labelled “D, E, L, I, H” were detected in the high energy scan. To have a better view of the qualitative detectability of the reported indications, the CT slices of the cube are shown in Figure 4.

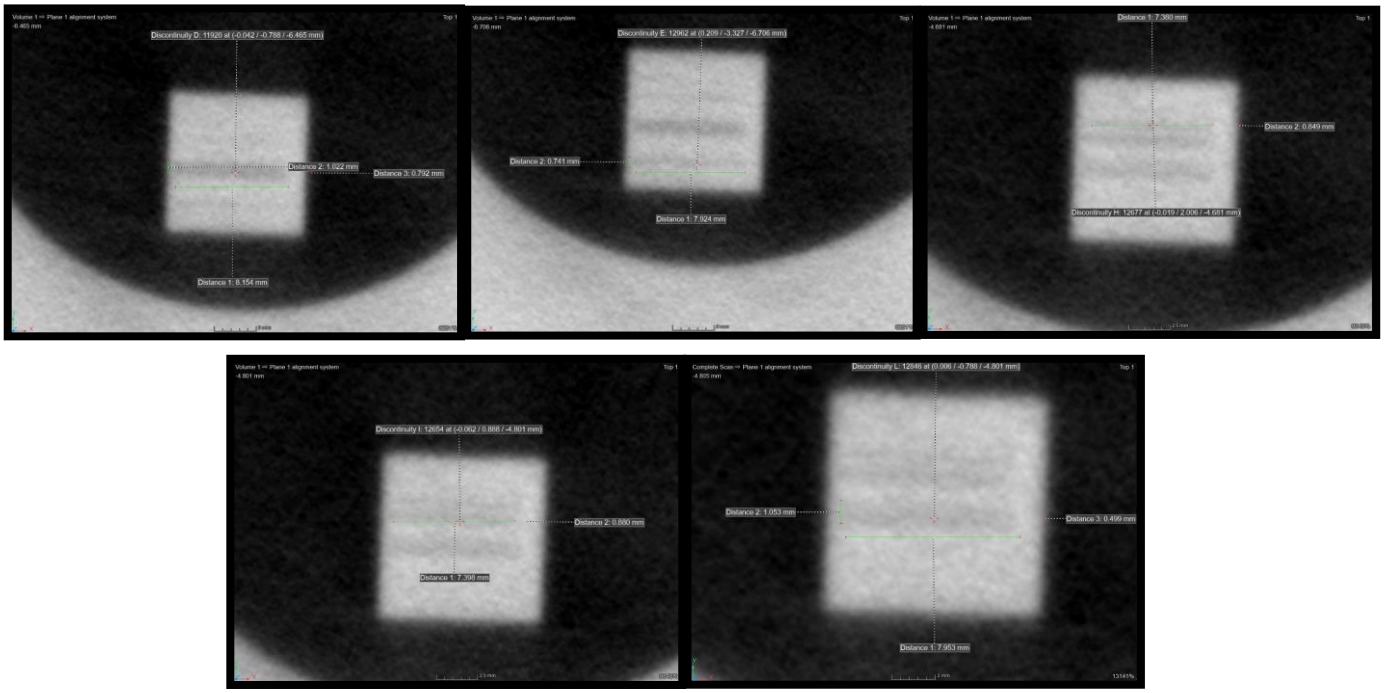

Figure 4 - CT cross sections of the RQI cube high energy scan. From left to right and top to bottom, indications: D, E, H, I, L

As expected, considering the nature of the high energy CT, a lower sharpness level is noticeable, as well as a higher noise level compared with medium energy CT. However, it is still possible to detect the major discontinuities that were introduced in the cube. It’s important to note that the contrast between the inside of the defects and the RQI material is limited because the defects are full of unfused powder, as the micro-CT scan revealed. For titanium alloys the unfused powder can be considered as half density of the plain material (correctly melted). Titanium alloys tend to have more spherical unfused powder particles with respect to aluminium, and consequently larger air spaces between them. **[5]** However, this is just detectable in a microscopic scale, while when the voxel size has a size in the order of magnitude of >100µm, the artificial defects only show as an average of the grey values between the density of the powder material, and the density of the air. This is due to the partial voxel effect. **[1]** Consequently, considering the characteristics of the system and the scan conditions, this result can be considered satisfactory.

Nevertheless, with the aim to further improve the scan quality, a merging process between different volumes of the RQI is described in the next paragraph.

2.5.3 RQI scan quality improvement via volume merging (voxel averaging)

Between the sources of defects detectability disturbance, the main ones can be identified as blurring, noise, and artifacts such as beam hardening and Compton scattering (due to the part and inside the DDA). **[7]**. These, if not attenuated, will produce a low contrast and noisy reconstruction. **[1]** As stated previously, this specific scan showed qualitatively a globally low level of artifacts. Additionally, because image sharpness on this kind of system has specific limits, it was chosen to try to improve the noise level of the reconstructed volume. In order to achieve this, two ways could have been followed:

- Radiographs frame averaging during the acquisition: by averaging the radiographs during the acquisition phase, it is possible to obtain noise reduction directly from the beginning of the process. However, this approach should be performed with a step scan acquisition, resulting in a considerable increase in scan time (starting from four times the standard scan time, and increasing depending on the number of frames averaged).

- Volume merging: this approach consists in scanning the region of interest (ROI) twice (at least) with standard parameters (continuous scan, among all the others). The two scans can be identical, or the object can be moved between them, in order to change the eventual artefacts positions in the reconstructed volumes and the Compton scatter level. Then, the two reconstructed volumes are first aligned together. This step is usually performed using Best-Fit alignment, but other alignment types are possible. The alignment quality is of great importance, as misaligned volumes will

produced altered data if averaged together. After this first step, the gray values of the voxels are averaged. This produces a merged volume with a global lower noise level (comparable to what is obtainable with frame averaging) and with the additional benefits of CT artefacts averaging and much shorter scan time with respect to the step-scan acquisition. Because of these two additional improvements, this second approach was chosen.

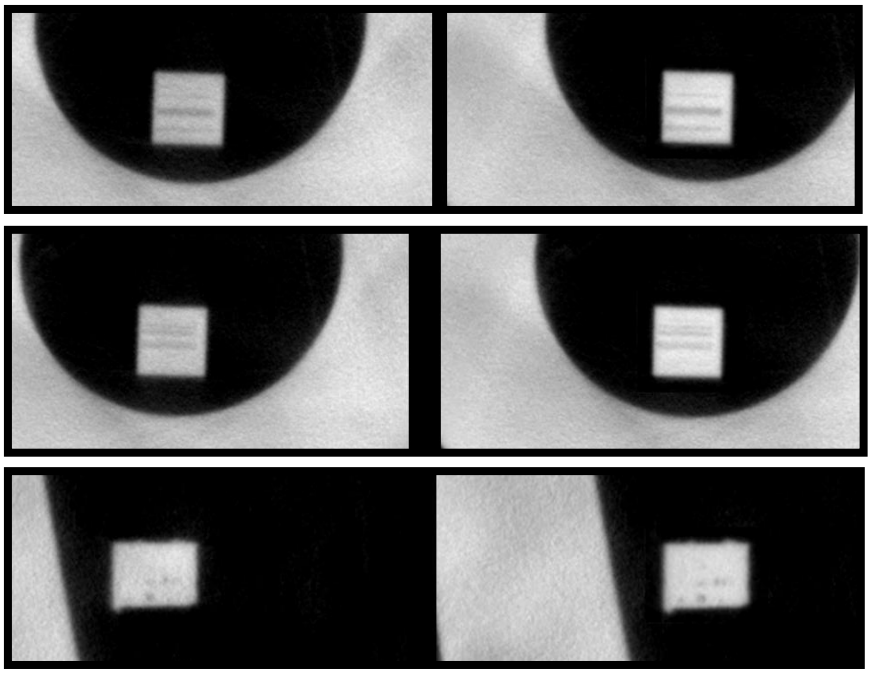

Figure 5 - CT slices showing the comparison between the "Standard" scan (left) and the "merged" scan (right)

In Figure 5 the CT slice comparison between the “standard” scan and the “merged” volumes is shown:

The side-by-side comparison reveals the lower noise level of the merged scan, which results in better definition of the defects borders. After a deeper analysis, it was concluded that the merged scan was able to detect three additional artificial defects labelled “B, G, O”, although they were judged at the limit of detectability.

To further substantiate these results, a Signal to Noise Ratio (SNR) measurement was performed in an area which was not interested by the artificial defects. As it can be seen in Figure 6, the “merged” scan show better SNR values respect to the “standard” scan:

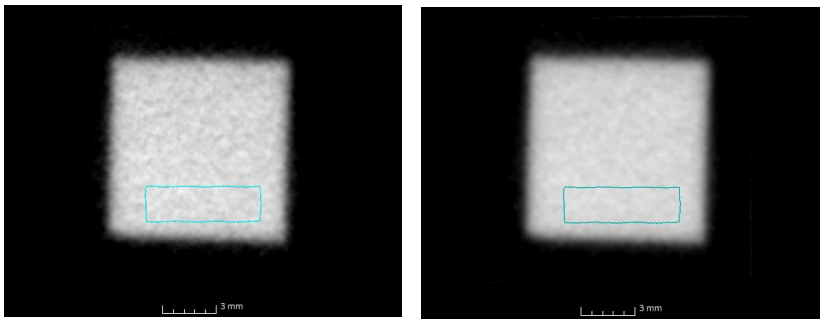

MEAN GREY VALUE: 37630 **STANDARD DEVIATION**: 979 **SNR**: 39	**MEAN GREY VALUE**: 37132 **STANDARD DEVIATION**: 514 **SNR**: 72

Figure 6 – Clean area of the RQI where the SNR measurement was performed with the related mean grey value, standard deviation, and SNR (left: "standard" scan, right: "merged" scan)

An additional way to quantify the scan quality could have been to measure Contrast to Noise Ratio (CNR). However, when it comes to measure the grey values inside small defects as the ones contained in the RQI, it is quite hard to create a region of

interest that nicely fits inside the defects, as generally it ends up always intercepting some of the material grey values, altering the results. Because of this, it was chosen not to perform the CNR measurement.

2.6 Application of artificial intelligence (AI) on CT slices

Artificial Intelligence can be defined as a set of techniques that allows to solve problems or perform tasks and activities that are typical of human abilities. In computer science this discipline deals with making machines able to make decisions independently, based on a circumscribed problem, by learning independently from the data provided through deep learning techniques and machine learning. **[12]** This ability has proven to be particularly suited when dealing with image recognition, where many specific features of an image can be detected by the algorithm and therefore recognized and categorized. **[13]** These images can also be extracted from CT volumes slices and processed by the AI with the aim to find specific features in them, such as differences in contrast that could represent a defect. Up to this day, the defect analysis activity has always been performed by human operators, but it comes with different limitations: in fact, when operators are involved, it actually becomes a subjective operation, dependant on the operator's judgement based on his/her experience and on the specific contrast variation visible on the computer screen representing the defects. This task is also quite demanding in terms of equipment requirements, where special rooms with controlled lighting and specific screen characteristics (the main ones being brightness and resolution, along with the ability to reproduce patterns described by SMPTE RP133) **[14]** play crucial role in how human vision can detect contrast variations. This activity, being highly repetitive and tiring for the eye, also requires constant concentration for a prolonged period of time. Therefore, human error must be accounted in the reliability of the analysis result.

Because of these limitations, when dealing with large batches of components, finding a way that could at least reduce the requirements and the possible sources of error during the analysis stage is desirable. With this target, TEC Eurolab developed a tailored software that, after exporting the reconstructed CT volumes into stacks of RAW images, performs an automated analysis based on the use of artificial intelligence, and generates a report containing all the anomalies that it detects.

The software is based on a deep learning model that processes these images and is trained in multiple ways both by comparing its results with previous reports generated on the same components by human users, and through feedback given by users on the results that the AI produces on new samples.

This application features a browser-based user interface, where the project manager can keep track of the global status of the analyses that are being processed by the AI algorithm. An example screenshot is reported in Figure 7, where the fully customized dashboard is shown.

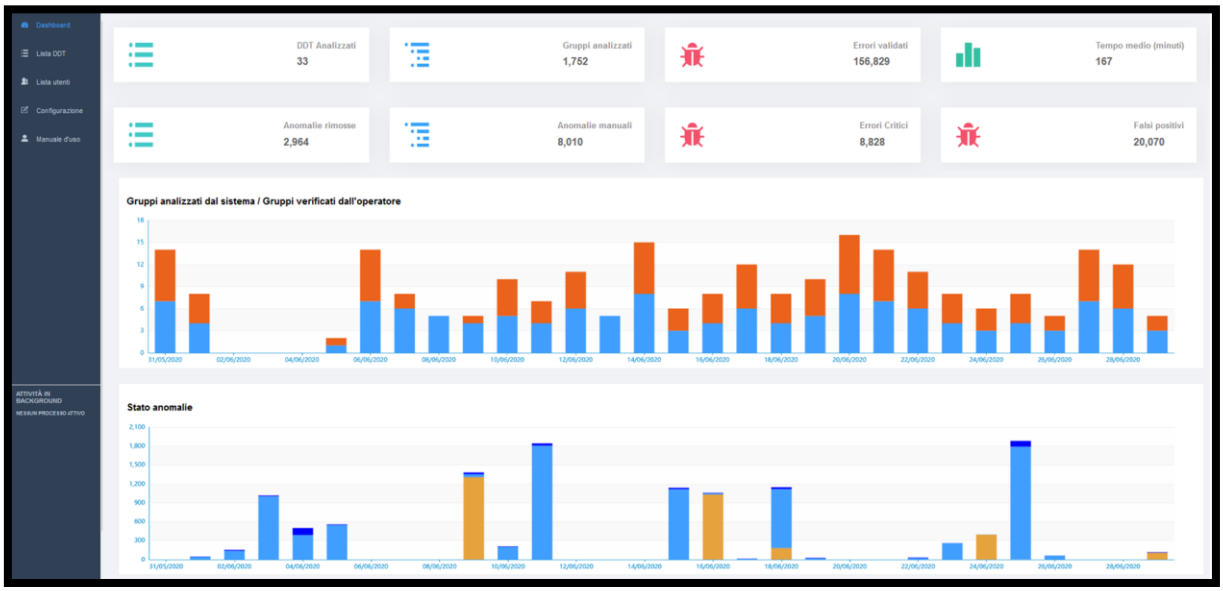

Figure 7 – Graphical User Interface (GUI) of the AI software. The histogram on the top show the number of analysed components for each day, while the one on the bottom shows the number of detected defects for each batch.

During the training period, using this interface it was also possible to keep track of the anomalies that were confirmed or discarded by user validation, while during production stage, it is possible to check the conformity for each batch of processed components.

When a closer look at the results is needed, the user can navigate to the exact CT slice that the AI algorithm classified as containing a defect, as shown in Figure 8, where a fully customized interface was developed.

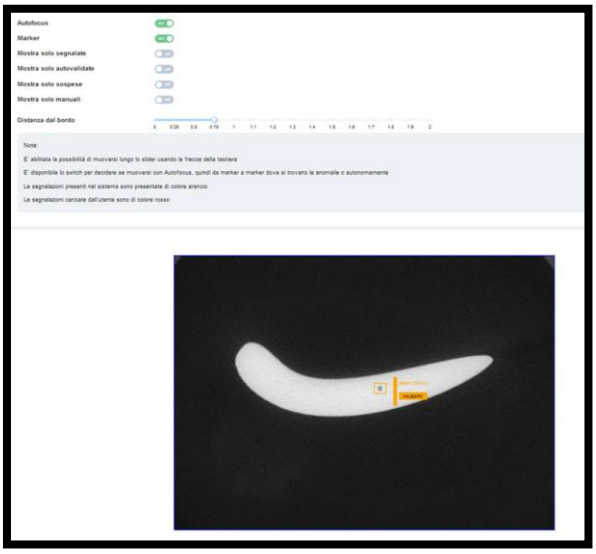

Figure 8 – Example of a slice processed by the AI where a defect was detected. Through the AI user interface it is possible to directly look at the CT slices where the algorithm detected a defect.

Sample Code	Defects	Found by AI and HU	Found only by AI	Found only by HU
1	17	13	4	0
2	13	6	7	0
3	11	5	6	0
4	6	1	4	1
5	7	5	2	0
6	11	6	3	2
7	6	1	4	1
8	4	1	2	1
9	19	8	11	0
10	13	3	7	3
11	14	4	10	0
12	14	6	7	1
13	13	2	11	0
14	10	4	4	2
15	11	7	4	0
16	5	3	2	0
17	10	1	8	1
18	7	5	2	0
19	13	6	7	0
20	9	2	5	2
21	10	4	6	0
22	13	5	7	1
23	14	8	6	0
24	19	7	12	0
25	6	3	3	0
26	8	5	3	0
27	5	2	2	1
28	18	7	9	2
29	9	5	4	0
30	21	10	11	0
31	15	10	3	2
TOTAL	351	155	176	20
%	***/***	**44,2**	**50,1**	**5,7**

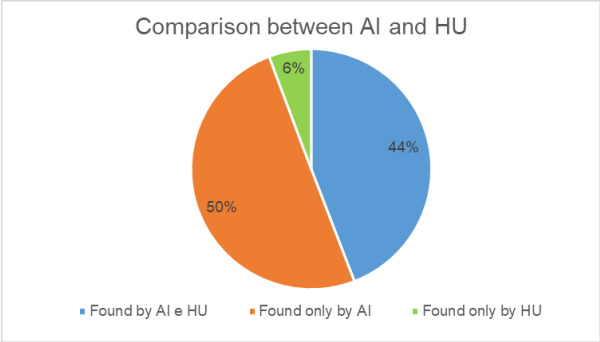

Figure 9 - Results obtained from the AI test run on a 31 samples batch.

To achieve this, a total sum of 4 million images and 250,000 labelled defects were used as training data. To fine tune the validation of the AI results, the technicians that oversaw validating the results, could log in with different privileges depending on their expertise in the analysis of that components. Based on the level of privileges, the validations that they performed on the AI reports, were considered with different weights for the neural network training. At the end of the development the software was tested on a real case scenario on a batch of 31 samples, and compared with the standard analysis procedure. The AI used the training data for the automatic analysis of the images of the samples, while the standard procedure consisted in defect analysis performed by a trained operator. The results shown that just 20 defects were found by human operator and not by the AI. It is

worth to mention that the AI was able to find 176 defects that were not detected by the human operator, as it can be seen in Figure 9. These defects however were not categorized as critical by the customer's acceptability criteria.

3 Results and discussion

The evaluation of the artificial defects detectability in an additively manufactured RQI, shielded by several centimeters of high-density TA6V alloy using a high energy CT system was performed. The output, when compared to the microfocus CT scan of the RQI alone, despite the expectable lower sharpness and increased noise levels due to the high energy system characteristics, show satisfactory results. These consist in the high energy system being able to detect linear indications with thicknesses in the order of 0.5mm and length of 8mm. These results have even higher relevance considering that the contrast between the inside of the defect and the RQI material is reduced due to the defect being full of unfused powder. The detectability and image quality were further improved by using volume merging (consisting in voxel averaging) producing an image with a reduced noise level, and averaged artifacts. The lower noise level was also quantified via SNR. This detectability result was achieved by specific technique development (tailored for high energy) and can be considered satisfactory when accounting for the characteristics of the system, especially the size of the focal spot and the detector SRB. This underlines how important the attention to scan parameters is, as it results in a reduction of the major CT artifacts (mainly being beam hardening, scattering and noise, while image sharpness is strongly dependent on the fixed characteristics of the system) and finally lead to the presented results. The CT volumes voxel averaging method showed to be applicable to this specific case, and suitable to be tested further, aiming to be extended in production use.

Finally, the tests that were conducted with TEC Eurolab AI software, produced the surprising result of 95% detection success, as shown in paragraph 2.6. This score was obtained comparing the results between the standard human control with the AI report just taking into account what was found out from the operator but not from the AI, without considering in the score what was found from the AI and not from the operator. This achievement underscores the effectiveness and potential of the AI-based defect analysis software. Furthermore, the comparison between the operator and the AI output has revealed that the software surpasses human operators in detecting defects, leading to a reduction in analysis time. By leveraging AI for defect analysis, the software significantly reduces the manual effort and time required for operators to perform these tasks. This enables operators to focus on critical decision-making activities and cooperate more efficiently with the AI system. The result is improved productivity, reduced operator fatigue, and enhanced job satisfaction.

4 Conclusion

The detectability of small linear indication (with reduced contrast because of the presence of unfused powder) with a minimum thickness of 0.5mm and 8mm length, was proven to be possible using a high energy system (featuring a 6 MeV linear accelerator as the X-Ray source). The first test shows that there is room for scan quality enhancement, using techniques such as volume merging. This kind of systems, still used quite rarely for production NDT inspections, proved to be capable of producing good detections results, but only when a careful scan parameter selection is used.

It was demonstrated that the use of AI can have a great impact in the application on CT volumes analysis, reducing inspection time and effort of the operators. Simultaneously, the analysis is less subjective to the experience of the operator and to the environment where the analysis is performed.

References

[1] S. Carmignato, W. Dewulf and R. Leach, Industrial X-Ray Computed Tomography, Springer International Publishing AG 2018, 2018.

[2] A. Horvatić Novak, B. Runje, Z. Keran and M. Orošnjak, "Image Artefacts in Industrial Computed Tomography," *TECHNICAL JOURNAL,* pp. 434-439, 2020.

[3] E. Sbettega, F. Zanini and S. Carmignato, "X-ray computed tomography for metal additive manufacturing: challenges and solutions for accuracy enhancement," *ScienceDirect,* pp. 114-118, 2018.

[4] C. Lemmer, "High Energy CT of a Rocket Nozzle Webinar," North Star Imaging, 08 July 2022. [Online]. Available: https://4nsi.com/high-energy-ct-of-a-rocket-nozzle-webinar/.

[5] A. Tawfik, M. Radwan, M. A. Attia, P. Bills, R. Racasan and L. Blunt, "The Detection of Unfused Powder in EBM and SLM Additive Manufactured Components," *Int. J. of Automation Technology,* p. Vol.14 No.6, 2020.

[6] J. P. Davim, A. Riveiro and J. Pou, Handbooks in Advanced Manufacturing - Additive Manufacturing, Eskisehir Osmangazi University, Eskisehir, Turkey: Elsevier, 2021.

[7] A. -. A. S. f. T. a. M. International, *E1441-19 - Standard Guide for Computed Tomography (CT)*, 2019.

[8] M. Maulin, P. G. Allinei, D. Eck, N. Estre, E. Payan, D. Tisseur and G. Kessedjian, *Characterization of the X-ray spectrum of a Linear Accelerator,* ANIMMA - EPJ Web of Conferences 253, 04002, 2021.

[9] D. Tisseur, N. Bhatia, N. Estre, L. Berge and E. Payan, "Evaluation of a scattering correction method for high energy tomography," in *EPJ Web of Conferences 170, 06006*, 2018.

[10] B. Kratz, F. Herold, J. C. Robbins and J. Tamm, *Study on the Influence of Scattered Radiation and the Usage of Scatter Reduction Methods for Computed Tomography,* Leuven, Belgium: 7th Conference on Industrial Computed Tomography, (iCT 2017), 2017.

[11] Y. Yanga, Y.-C. Wua, L. Lic, S.-Y. Zhangc, K.-G. Donga, T.-K. Zhanga, M.-H. Yua, X.-H. Hanga, B. Zhua, F. Tana, Y.-H. Yana, G. Lia, W. Fana, F. Lua, Z.-Q. Zhaoa, W.-M. Houa, L.-F. Caoa and Y.-Q. Gu, "Design and characterization of high energy micro-CT with a laser-based Xray source," *Results in Physics - Elsevier,* 2019.

[12] V. V. Shakirova, K. P. Solovyevaa and W. L. Dunin-Barkowskia, "Review of State-of-the-Art in Deep Learning Artificial Intelligence," *Optical Memory and Neural Networks,* pp. 65-80, 2018.

[13] Y. TIAN, "Artificial Intelligence Image Recognition Method Based on Convolutional Neural Network Algorithm," *IEEE Access,* p. Volume 8, 21 July 2020.

[14] L. Yenumula, R. V. Acharya, U. Kumar and A. Dash, *Performance Evaluation of Industrial Computed Radiography Image Display System,* Bhabha Atomic Research Centre, Mumbai – 400085, India: Industrial Tomography and Instrumentation Section, Isotope Production and Applications Division, 2016.